remote sensing

MDPI

Article

Drone-Based Imaging Polarimetry of Dark Lake Patches from the Viewpoint of Flying Polarotactic Insects with Ecological Implication

Dénes Száz [1], Péter Takács [1,2], Balázs Bernáth [1,2], György Kriska [3,4], András Barta [1,5], István Pomozi [1,2] and Gábor Horváth [1,*]

[1] Environmental Optics Laboratory, Department of Biological Physics, ELTE Eötvös Loránd University, Pázmány Sétány 1, H-1117 Budapest, Hungary
[2] Drem Innovation and Consulting Ltd., Szentendrei út 95, H-1033 Budapest, Hungary
[3] Group for Methodology in Biology Teaching, Biological Institute, ELTE Eötvös Loránd University, Pázmány Sétány 1, H-1117 Budapest, Hungary
[4] Centre for Ecological Research, Institute of Aquatic Ecology, Karolina út 29-31, H-1113 Budapest, Hungary
[5] Estrato Research and Development Ltd., Németvölgyi út 91/c, H-1124 Budapest, Hungary
* Correspondence: gh@arago.elte.hu

Abstract: Aquatic insects detect water by the horizontal polarization of water-reflected light and thus are attracted to such light. Recently, in the Hungarian Lake Balaton we observed dark water patches forming between every autumn and spring because of the inflow of black suspended/dissolved organic matter into the bright lake water. Earlier, the polarization characteristics of such water surfaces were mapped by imaging polarimeters from the ground. In order to measure the reflection-polarization patterns of these dark lake patches from the higher viewpoint of flying polarotactic aquatic insects, we designed a drone-based imaging polarimeter. We found that the dark lake patches reflected light with very high ($60\% \leq d \leq 80\%$) degrees of horizontal polarization at the Brewster's angle, while the bright lake water was only weakly ($d < 20\%$) horizontally polarizing. There was a large contrast in both the radiance and degree of polarization between dark lake patches and bright lake water, while there was no such contrast in the angle of polarization. The ecological implication of these findings could be that these dark lake patches attract water-seeking polarotactic insects, which may oviposit more frequently in them than in the brighter lake water. However, it might not matter if they lay their eggs in these dark patches rather than the bright lake water, because this may simply increase the abundance of breeding flying insects in areas where dark patches are common.

Keywords: polarization; imaging polarimetry; drone; water surface; aquatic ecology

Citation: Száz, D.; Takács, P.; Bernáth, B.; Kriska, G.; Barta, A.; Pomozi, I.; Horváth, G. Drone-Based Imaging Polarimetry of Dark Lake Patches from the Viewpoint of Flying Polarotactic Insects with Ecological Implication. *Remote Sens.* **2023**, *15*, 2797. https://doi.org/10.3390/rs15112797

Academic Editors: Javier Leon, Daniel L. Harris and Stephanie Duce

Received: 29 March 2023
Revised: 20 May 2023
Accepted: 22 May 2023
Published: 27 May 2023

1. Introduction

In the 1980s, Rudolf Schwind discovered that aquatic insects detect water bodies by means of the horizontal polarization of water-reflected light in species-dependent spectral (ultraviolet, blue, or green) ranges [1–8]. After his pioneering studies, many water-loving insect species were found to possess positive polarotaxis, which is a strong attraction to horizontally polarized light [9–18] in such a way that a higher degree of linear polarization results in stronger visual attraction [19].

Because of their evolutionarily developed polarotaxis, these insects can be deceived by artificial surfaces reflecting highly (i.e., with a high degree of polarization) and horizontally polarized light. This visual deception of aquatic insects was first observed at the crude oil lakes in the desert of Kuwait, when they landed and perished on highly and horizontally polarizing shiny black oil surfaces [20]. An ecological analogy to these oil lakes is a Hungarian open-air oil lake in which numerous aquatic insects and birds, which were attracted by the shiny surfaces, perished in large masses for more than 50 years [21].

These insects were predominantly associated with water and attracted to the horizontally polarized oil-reflected light. A similar phenomenon was observed on asphalt roads where mayflies laid their eggs en masse instead of returning to the creek running parallel to the horizontally polarizing, dark grey road surface [22].

This maladaptive behaviour of polarotactic insects has led to the concept/term of polarized light pollution (PLP), meaning all the harmful effects of highly and horizontally polarized light reflected from smooth and dark artificial surfaces on polarotactic water-loving insects [16]. The most typical horizontal sources of PLP are crude oil spills/ponds/lakes [20,21], asphalt roads [22], and black plastic sheets used in agriculture [21]. Because of the mentioned behavioural maladaptation, these manmade surfaces function as evolutionary/ecological traps for polarotactic insects [23–27].

Since the effects of PLP (i.e., perishing of adults and/or oviposited eggs on the inadequate artificial substrate that mimics the water surface by the reflected horizontal polarization) are dangerous for the offspring generation of polarotactic water insects, using imaging polarimeters from a low height ($h < 1.5$ m) above the ground, researchers have systematically mapped the PLP sources and compared them with different natural water surfaces (reviewed in [16]). In the past few years, we observed dark water patches of the Hungarian Lake Balaton forming periodically between every autumn and spring because of the inflow of dark-coloured canal/river waters containing dissolved and suspended black organic matter originating from dead fallen leaves of forests (Figure 1). In order to measure the reflection-polarization characteristics of these dark lake patches from the higher ($h > 1.5$ m) viewpoint of flying polarotactic insects, we equipped a drone with a linear polarization camera. In this work, we present the polarization characteristics of these dark lake patches recorded by drone polarimetry and discuss their possible visual–ecological implication. Noticeably, because of their very high ($60\% \leq d \leq 80\%$) degrees of horizontal polarization at the Brewster's angle, these dark lake patches are optically similar to certain dark PLP sources. However, the former are ecologically suitable and advantageous for aquatic insects and their eggs and larvae, in contrast to the latter.

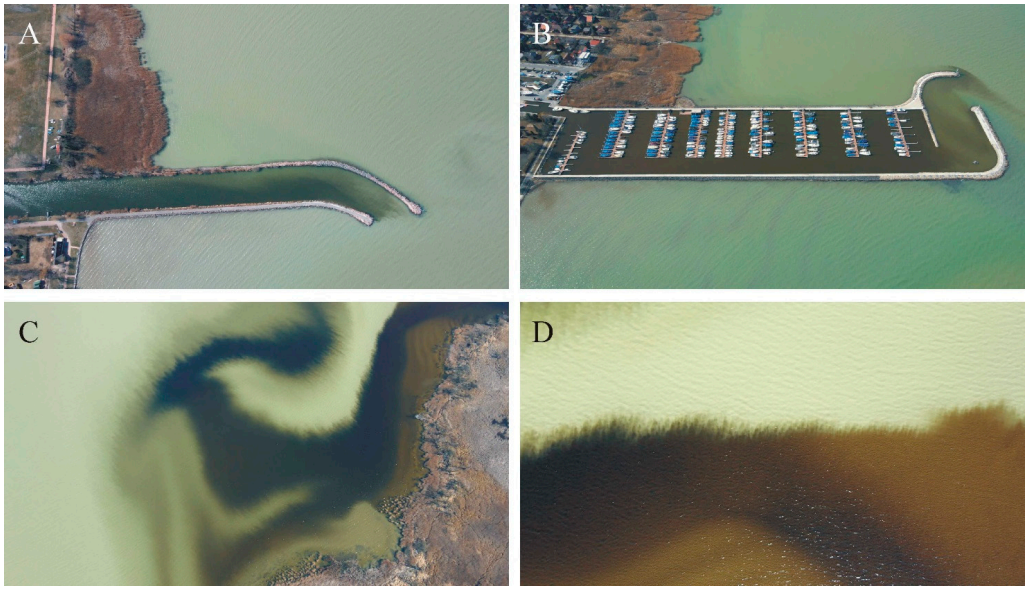

Figure 1. Pictures of dark water patches in the Lake Balaton at the (**A**) harbour of Balatonmariafurdo (46°42′22″N, 17°22′14″E), (**B**) Balatonfenyves (46°42′39″N, 17°28′40″E), and (**C**,**D**) estuary of the River Zala (46°42′21″N, 17°15′53″E) taken from a drone on 3 May 2022 between 12:00 and 16:00 h (=local summer time = UTC + 2 h).

2. Materials and Methods

2.1. Study Sites

We performed our drone polarimetric measurements at three study sites close to the shore of the Hungarian Lake Balaton where the dark lake patches occur from autumn to spring because black humic canal water mixes with the lake water.

(1) The first study site was at the harbour of Balatonmariafurdo (46°42′22″N, 17°22′14″E), where two concrete walls surrounded the inflowing canal water from two sides. The harbour water mixed with the lake water through a thin canal used by boats/yachts. The canal mouth was at the base of the harbour, where water inflow was controlled by a water gate.

(2) The second site was at the estuary of the River Zala (46°42′21″N, 17°15′53″E), where it flows into Lake Balaton. Since the river water stems from the same area as the canal water in site 1, its colour is also black between autumn and spring owing to rich humic substances.

(3) The third site was the harbour of Balatonfenyves (46°42′39″N, 17°28′40″E) (46°42′54.693″N, 17°28′33.413″E), which also had an elongated water body separated from the lake by two parallel, 400 m long concrete dykes. The dark harbour water mixed with the bright lake water through a boat/yacht canal.

At locations 1 and 3, from autumn to spring, the canal transports dark water with a high concentration of dissolved humic substances; thus, the colour of the harbour water is almost black. The lake water is, however, significantly brighter and has a greenish-yellowish colour. Thus, there is a striking darkness/brightness contrast between the harbour water and lake water. After closing the water gate in May, because of the currents and boat traffic, the colour of the harbour water starts to lighten and from the end of July no colour difference occurs between the harbour and lake waters.

2.2. Drone-Based Imaging Polarimetry

The reflection-polarization characteristics of water bodies at the three study sites were measured with drone polarimetry in the red (650 $\pm$ 50 nm), Green (550 $\pm$ 50 nm) and Blue (450 $\pm$ 50 nm) parts of the spectrum. The measurements were performed on 3 May 2022 under clear or partly cloudy sky conditions between 12:00 and 16:00 h (=local summertime = UTC + 2 h). Using a linear polarization camera installed on the drone, we captured a linear polarization image every two seconds of a target (a dark water patch). After evaluation of the polarization images, we obtained the patterns of the radiance I, degree of linear polarization d, and angle of polarization α in the R, G and B spectral ranges. From the I_R, I_G, and I_B patterns a colour picture was composed showing the target as seen without a linear polarizer.

Drone: The drone model was a DJI Matrice 210 v2 RTK. The drone had GPS positioning, remotely controlling the yaw, pitch, and roll angles as well as the height. In the computer evaluation of the polarization images taken by the camera, these data provided by the drone were used.

Linear polarization camera: For imaging polarimetric measurements we used a Colour GigE (DYK 33GX250) Polarsens® industrial camera (vendor: Basler, Ahrensburg, Germany) with a Sony Pregius S™ polarisation-sensitive CMOS sensor (IMX250MYR) with the following technical specifications: dynamic range = 12 bit, resolution = 5 MP = 2448 (vertical subpixel columns) $\times$ 2048 (horizontal subpixel rows), frame rate = 24/s, video output format = 8-bit polarized Bayer, 12-bit polarized Bayer packed, 16-bit polarized Bayer, electrical interface = gigabit ethernet (RJ45). Its optical interface had the following characteristics: infrared cut filter, format = 2/3 inch, shutter = global, subpixel size = 3.45 μm (horizontal) $\times$ 3.45 μm (vertical), shutter = 20 μs. The diameter D, focal length f and circular field of view δ of the objective lens (type: Basler Lens C125-0418-5M-P-f4 mm, vendor: Basler) were D = 29 mm, f = 4 mm, $\delta = 86°$.

Figure 2 shows schematically the lens and sensor layer of the linear polarization camera. A superpixel of the sensor layer composed of four pixels (1 red + 2 green + 1

blue) corresponded to a subpixel of the image (2448 × 2048) taken by the camera. The camera used an on-chip polarization technology, which means that at each quadripartite superpixel, one of the four directional built-in linear polarizers was applied with transmittance directions of 90° (top left quartile), 135° (top right), 0° (bottom left), and 45° (bottom right) from the vertical (Figure 2) in the normal orientation of the camera, that is, when the top and bottom walls of its house were horizontal, this resulted in four subpixels next to each other creating a superpixel. Thus, four linear polarization images (2448 × 2048) were captured simultaneously without the need for a rotating linear polarizer. The camera took one polarization image every 2 s. The spectral sensitivities of the red, green, and blue channels of the camera are shown in Figure 3.

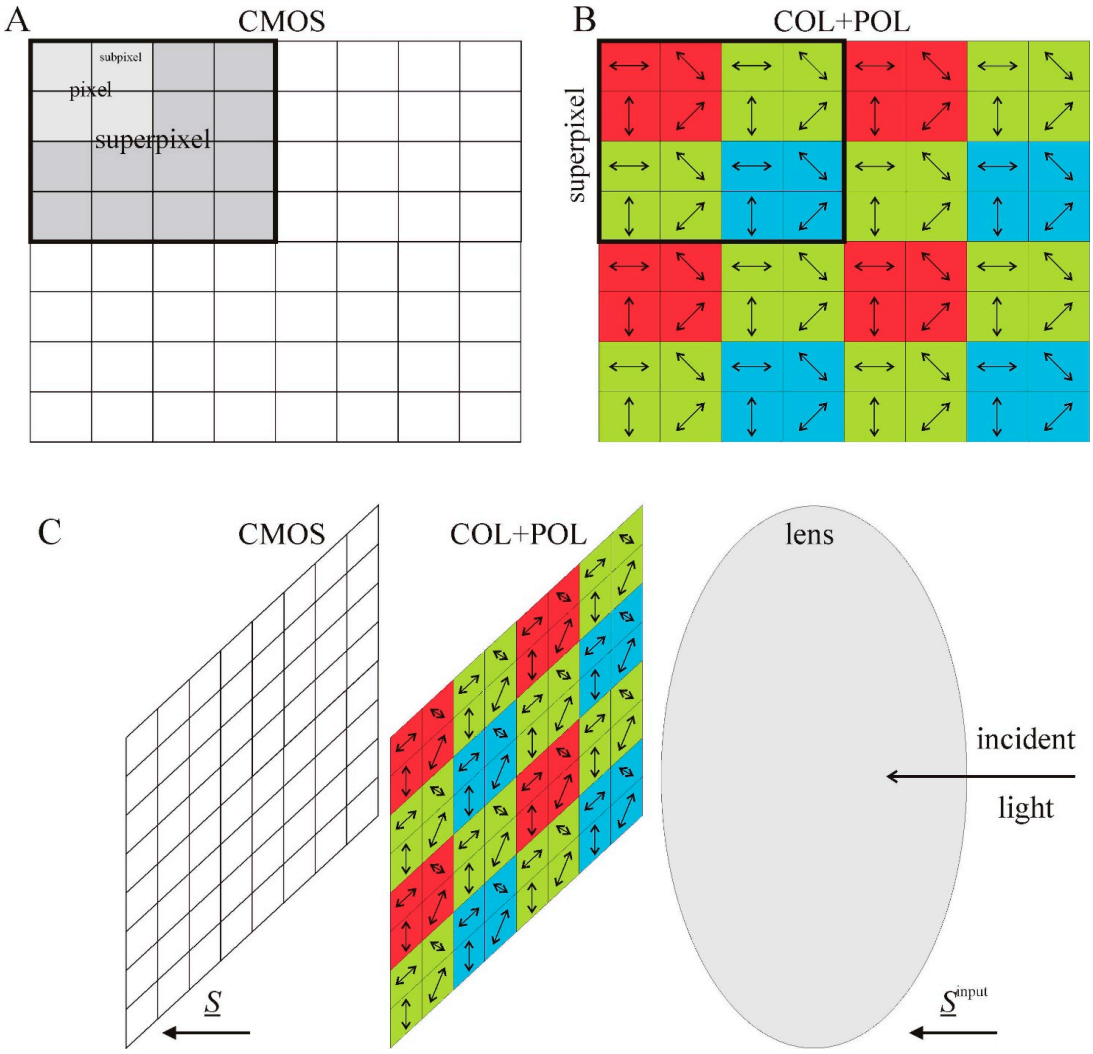

Figure 2. Schematic representation of the radiance-detecting CMOS sensor (**A**), the colour- (R: red, G: green, B: blue) and polarization-sensitive COL + POL filter (**B**), and the lens in front of the CMOS and COL+POL arrays of the linear polarization camera used for drone polarimetry (**C**). The double-headed arrows show the transmittance direction of linear polarizers. $\underline{S}$ is the Stokes vector of light. A superpixel is composed of four pixels: 1 R + 2 G + 1 B. A superpixel corresponds to a subpixel of the image (2448 × 2048) taken by the camera.

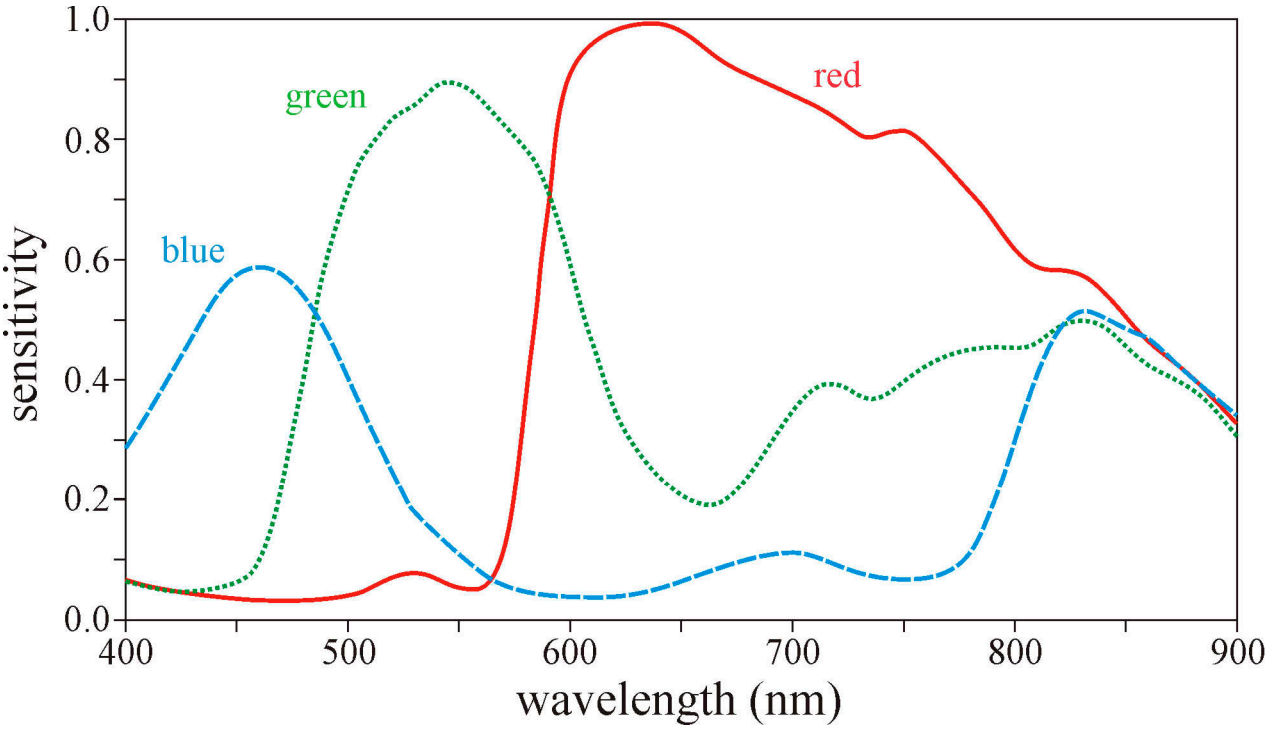

Figure 3. Spectral sensitivities of the red, green, and blue channels of the linear polarization camera used in drone-based imaging polarimetry.

The camera was installed on the bottom of the drone, and its optical axis pointed toward the Brewster's angle $\theta_{Brewster}$ = arctan (n = 1.33) = 53° relative to the vertical, where n = 1.33 is the refractive index of water (Figure 4). We chose $\theta_{Brewster}$, because from this direction unpolarized incident light is always reflected with a maximal degree of horizontal polarization, and water-seeking polarotactic aquatic insects detect water on the basis of this highly and horizontally polarized signal coming from the Brewster's angle [1,4,7,19].

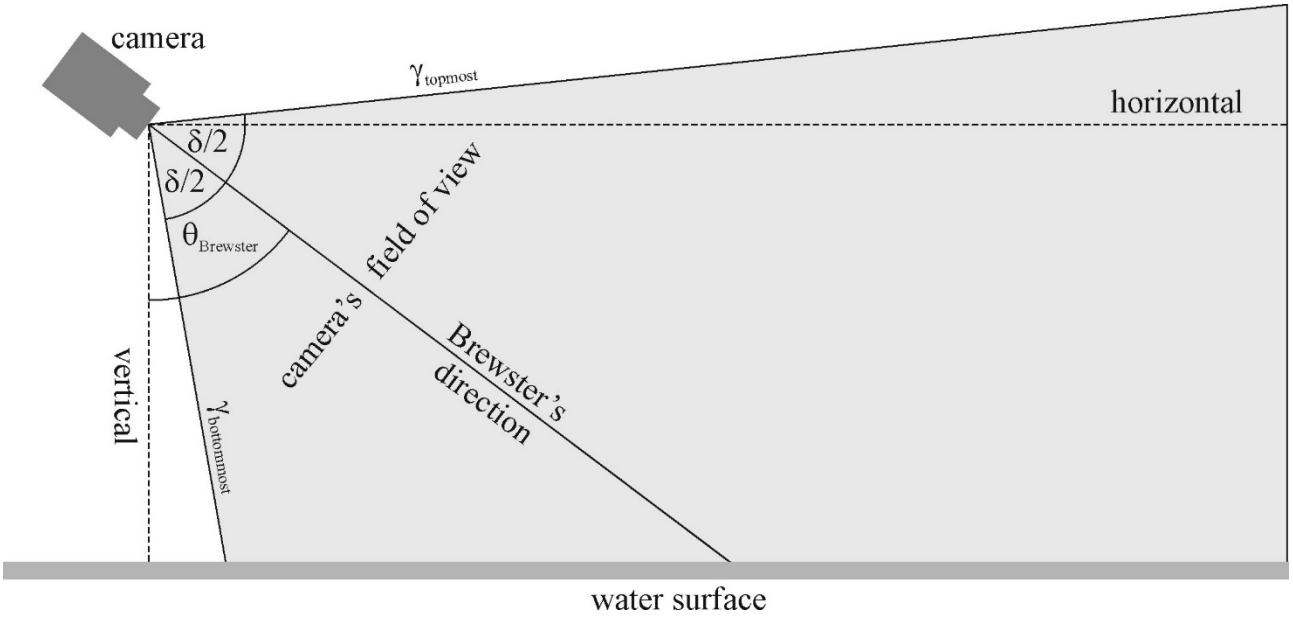

Figure 4. The optical axis of the polarization camera with a field-of-view angle δ = 86° on the water surface with Brewster's angle $\theta_{Brewster}$ = 53° from the vertical. $\gamma_{topmmost} = \theta_{Brewster} + \delta/2 = 96°$ and $\gamma_{bottommost} = \theta_{Brewster} - \delta/2 = 10°$ relative to the vertical.

Azimuth directions of the polarization camera: In our three measurement campaigns, we measured the reflection-polarization patterns of dark lake patches only in three relevant azimuth directions: slightly leftward from the solar meridian, slightly rightward from the solar meridian, and rightward, more or less perpendicularly to the solar meridian. These three directions of view of the drone-based polarization camera were enough to demonstrate the typical reflection-polarization characteristics of the dark lake patches studied. The position, orientation, and height of the drone-based imaging polarimeter were logged automatically by the drone's onboard Global Positioning System. In this work, the sun-to-drone angle of the optical axis of the polarization camera from the solar meridian is marked by β.

2.3. Evaluation of Polarization Images

Throughout this work, we used the following nomenclature for the two polarization variables: the degree (%) of linear polarization is marked by d, and the angle of polarization measured clockwise from the vertical is denoted by α.

For computer evaluation of the polarization images taken by the drone-based linear polarization camera, we used custom-written software that was created in Python programming language using the OpenCV algorithm package for image processing. Briefly, the evaluation process of the polarization images provided by the camera was the following: (i) Using the radiance values I_k (k = 1, 2, 3, 4) sensed by the four (R, G, G, B) pixels of a superpixel of the camera's sensor layer, we calculated the linear polarization Stokes vector $\underline{S}$ (without the fourth, circular polarization component) of light incident on the CMOS sensor at each subpixel of the raw image taken by the camera (Figure 2). (ii) We were interested in the input Stokes vector $\underline{S}^{\text{input}}$ of light incident on the optics (Figure 2C). Using the linear polarization Mueller matrix $\underline{\mathbf{M}}$ of the optics (sensors + lens), the Stokes vector incident on the CMOS sensor is $\underline{S} = \underline{\mathbf{M}}\underline{S}^{\text{input}}$. From this, the input Stokes vector $\underline{S}^{\text{input}} = \underline{\mathbf{M}}^{-1}\underline{S}$ was calculated, where $\underline{\mathbf{M}}^{-1}$ is the inverse of Mueller matrix $\underline{\mathbf{M}}$. (iii) The input radiance I, degree of linear polarization d, and angle of polarization α of light incident on the optics were calculated as follows: $I = S_0$, $d = \sqrt{S_1^2 + S_2^2}/S_0$, $\alpha = 0.5\arctan(S_2/S_1)$, where S_0, S_1 and S_2 are the three linear polarization components of the input Stokes vector $\underline{S}^{\text{input}}$. Our camera detected only linear polarization, which was, however, not a problem, because aquatic insects are not sensitive to circular polarization [1–19]. (iv) Finally, the I-, d- and α-patterns were visualised as two-dimensional colour-coded maps.

In a test of the polarization camera and evaluation of its polarization images, we measured the values of the degree of linear polarization d and angle of polarization α of light transmitted through a linearly polarizing sheet (P-ZN/R-12628, Schneider, Bad-Kreuznach, Germany) with different transmission directions (0°, 45°, 90°, 135° from the vertical). According to this test, the uncertainties of the measured d- and α-values were $\pm$1% and $\pm$1° for d = 100%, respectively, while for d = 15% (=threshold of polarization sensitivity of aquatic insects [19]), the uncertainties increased to $\pm$3% and $\pm$3°.

3. Results

The polarization patterns measured in the red (650 nm), green (550 nm), and blue (450 nm) parts of the spectrum are shown in Figure 5 (and Supplementary Figures S1–S8). In Figures 6–8 we present the polarization patterns measured only in the blue (450 nm) spectral range, because the majority of aquatic insects sense the polarization of water-reflected light in the short (blue or ultraviolet) wavelength range [1,7,8,18,19,26]. From these figures it was clear that in the visible spectrum ($400 \leq \lambda \leq 700$ nm) the reflection-polarization characteristics of the studied water bodies depended only slightly on the wavelength λ, therefore these patterns were very similar in the blue, green, and red ranges. Although our polarization camera was not sensitive to the ultraviolet range (UV: 250 nm $< \lambda <$ 400 nm), this was not a problem because the UV polarization patterns of the water surface should be close/similar to those in the blue range.

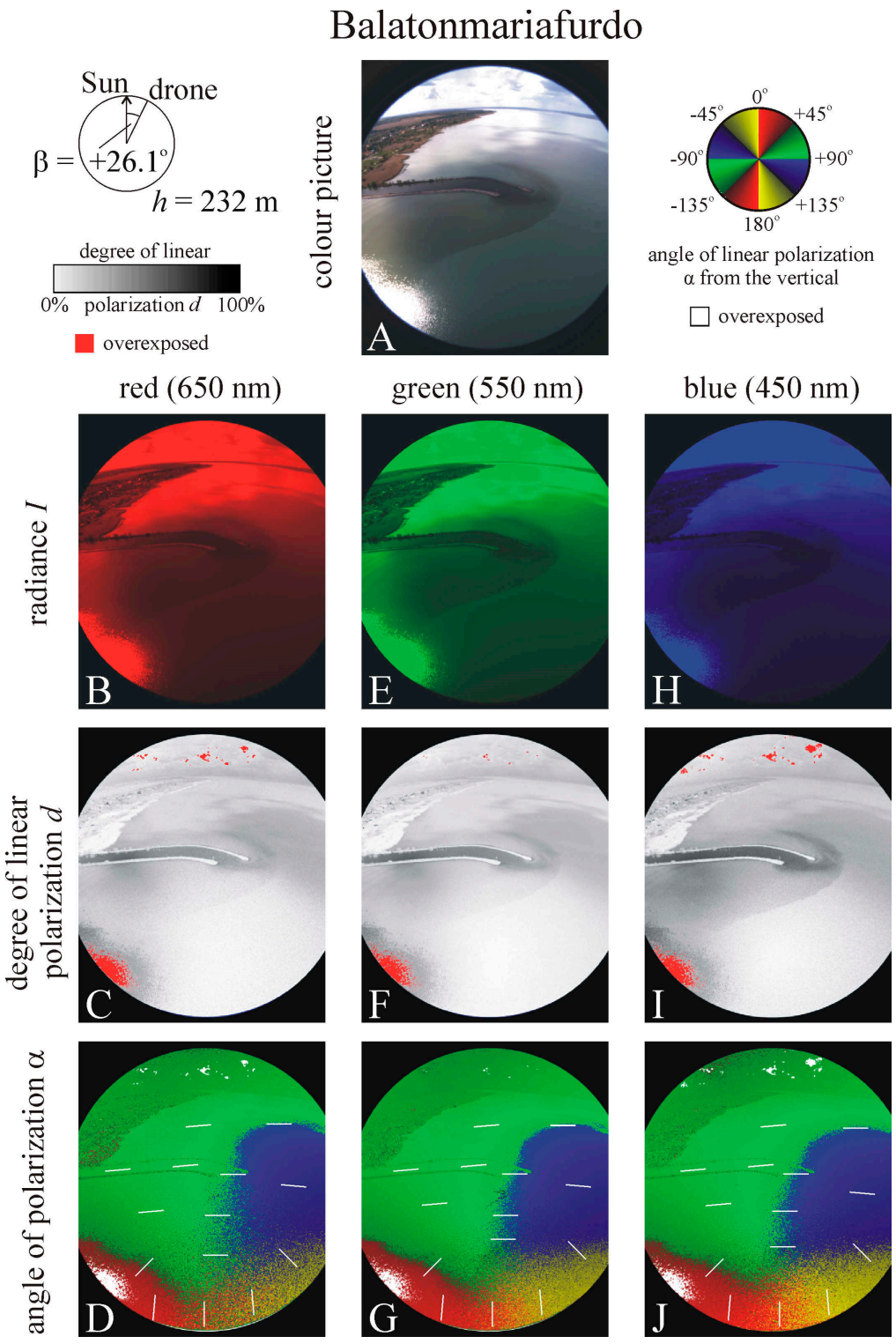

Figure 5. Colour picture (**A**) and patterns of the radiance I (**B**,**E**,**H**), degree of linear polarization d (**C**,**F**,**I**) and angle of polarization α (**D**,**G**,**J**) of Lake Balaton at the harbour of Balatonmariafurdo (46°42′22″N, 17°22′14″E) measured with drone-based imaging polarimetry from height h = 232 m in the red (650 nm), green (550 nm), and blue (450 nm) spectral ranges on 3 May 2022 at 13:46:07 (=UTC + 2 h). In the α-patterns the white bars show the local directions of polarization. The azimuth angle of the drone's optical axis is β = +26.1° clockwise from the solar meridian.

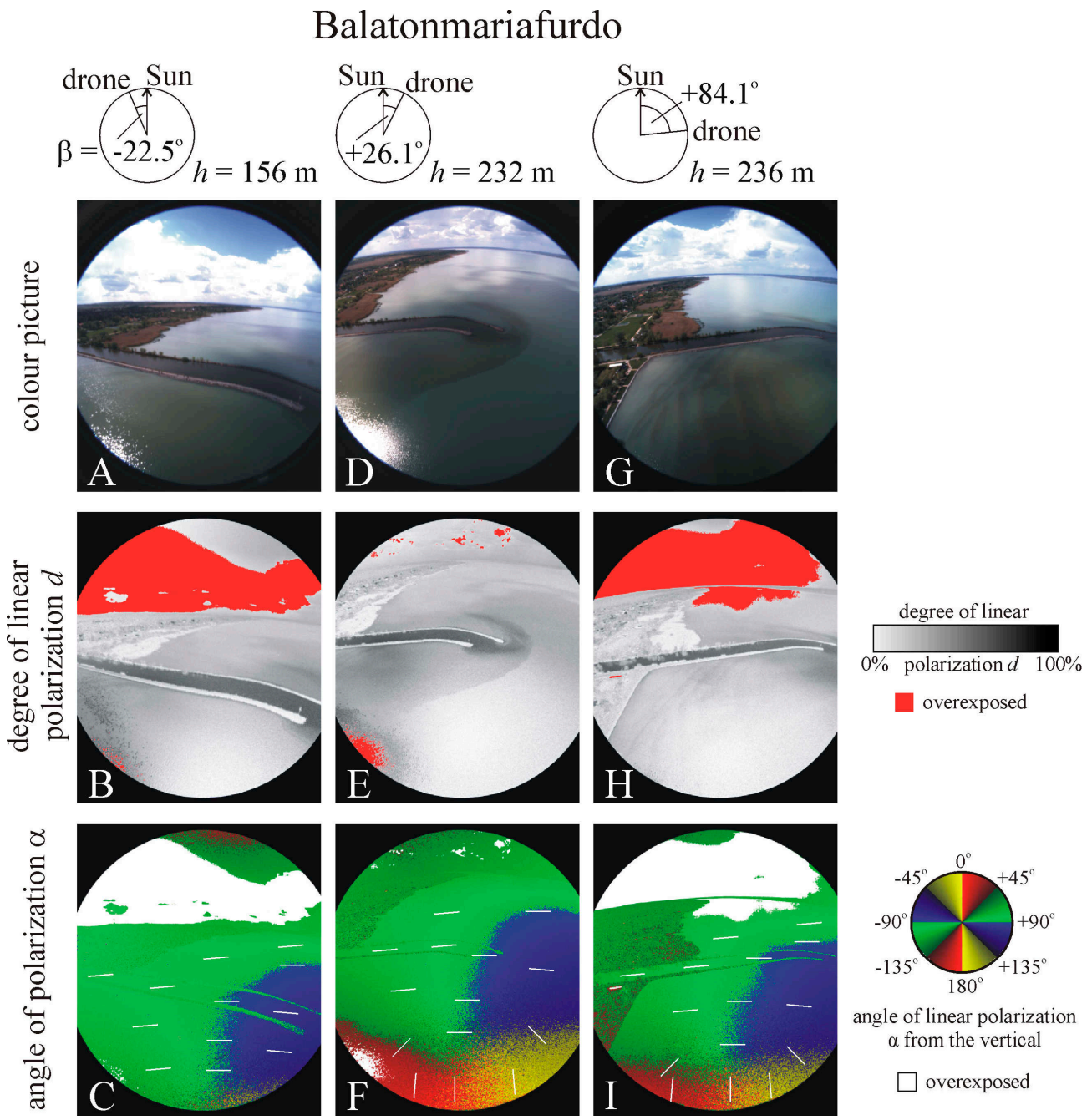

Figure 6. Colour picture (**A**,**D**,**G**) and patterns of the degree of linear polarization d (**B**,**E**,**H**) and angle of polarization α (**C**,**F**,**I**) of Lake Balaton at the harbour of Balatonmariafurdo (46°42′22″N, 17°22′14″E) measured with drone-based imaging polarimetry in the blue (450 nm) spectral range from three different heights (h = 156, 232, 236 m) and azimuth angles ($\beta = -22.5°$, +26.1°, +84.1° clockwise from the solar meridian) of the drone's optical axis on 3 May 2022 at 13:48:13, 13:46:07, and 13:42:23 (=UTC + 2 h), respectively. In the α-patterns the white bars show the local directions of polarization.

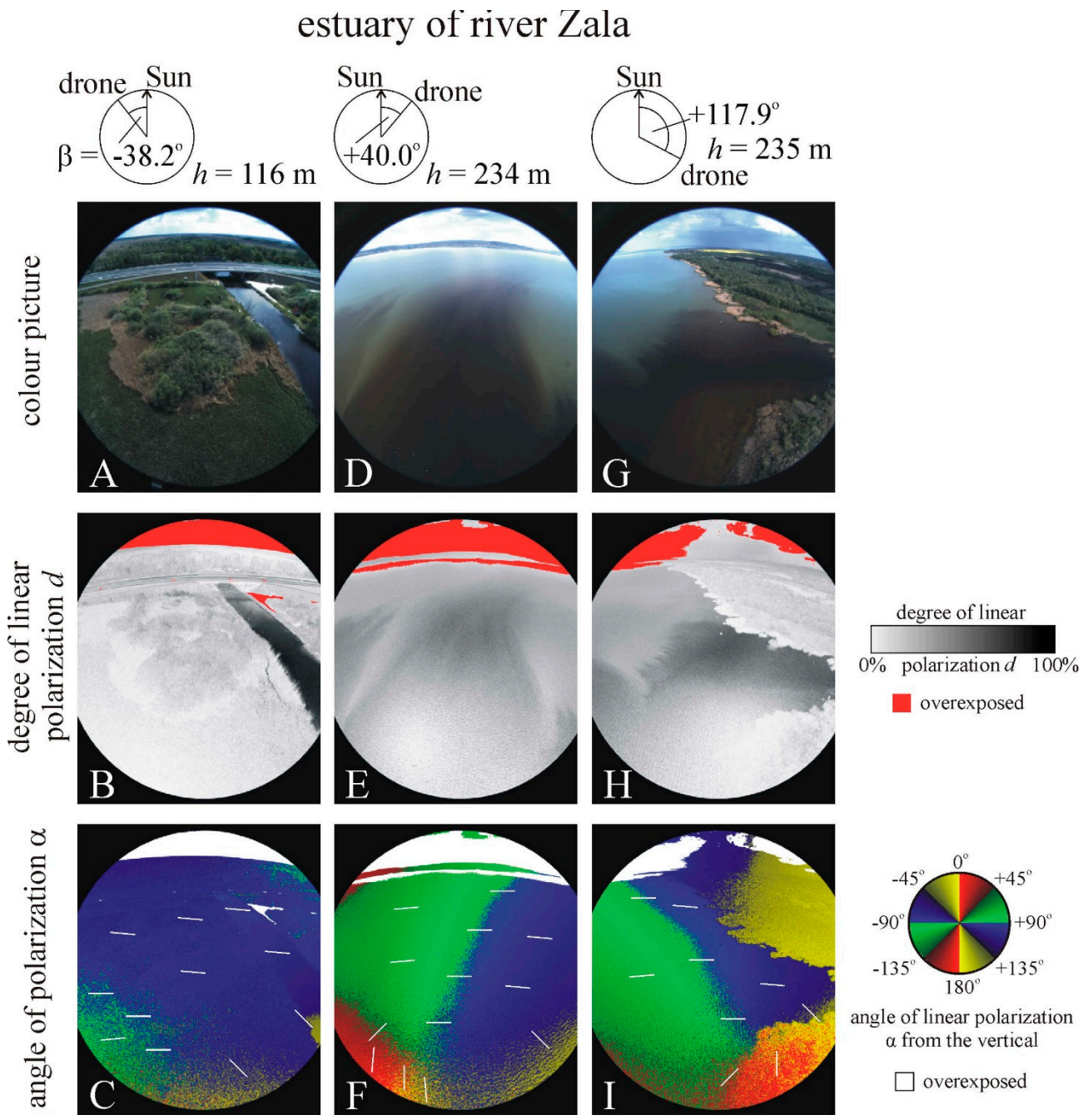

Figure 7. Colour picture (**A**,**D**,**G**) and patterns of the degree of linear polarization *d* (**B**,**E**,**H**) and angle of polarization α (**C**,**F**,**I**) of Lake Balaton at the estuary of the River Zala (46°42′21″N, 17°15′53″E) measured with drone-based imaging polarimetry in the blue (450 nm) spectral range from three different heights (*h* = 116, 234, 235 m) and azimuth angles (β = −38.2°, +40.0°, +117.9° clockwise from the solar meridian) of the drone's optical axis on 3 May 2022 at 15:06:46, 15:02:14 and 15:00:46 (=UTC + 2 h), respectively. In the α-patterns the white bars show the local directions of polarization.

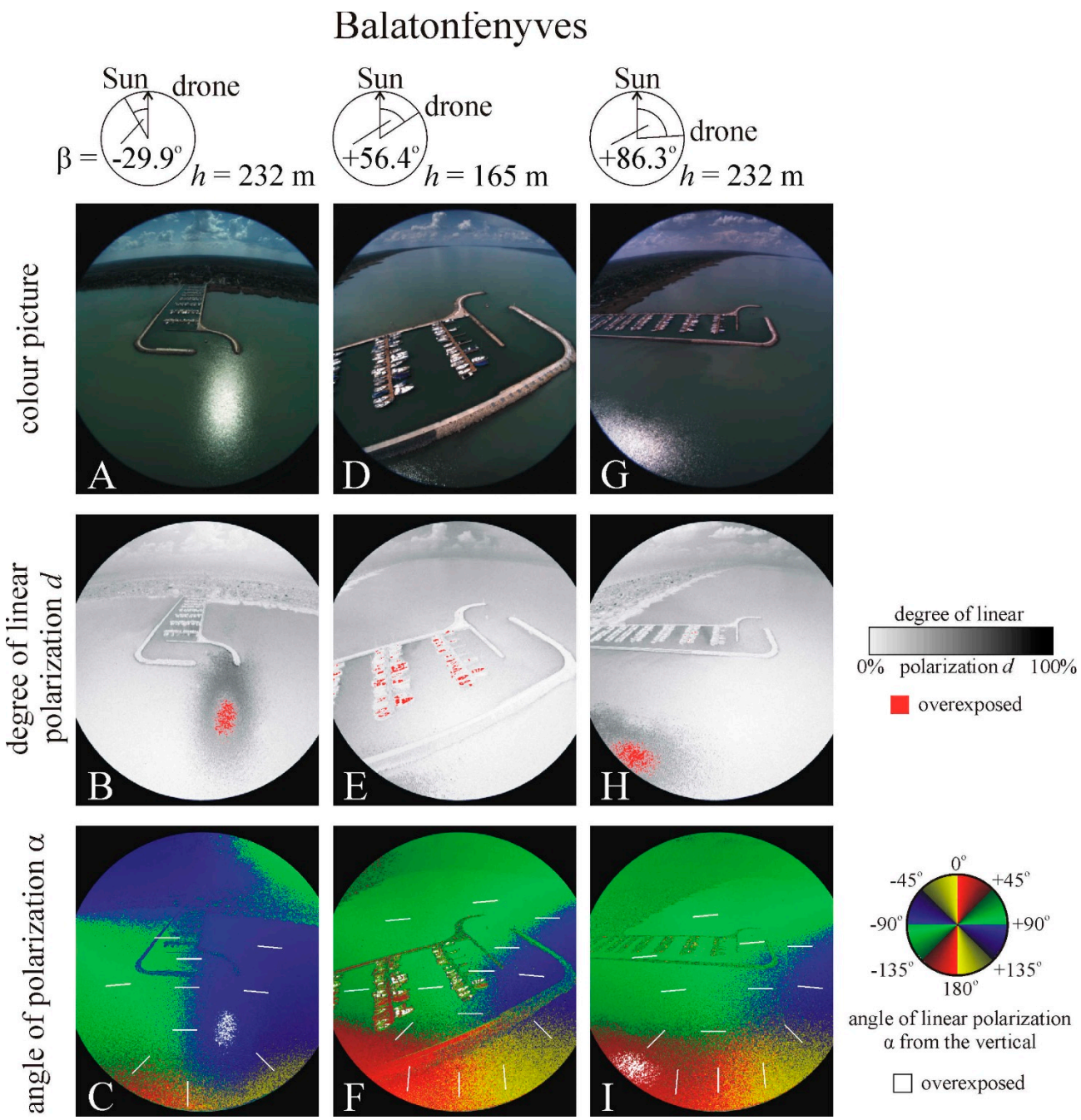

Figure 8. Colour picture (**A**,**D**,**G**) and patterns of the degree of linear polarization d (**B**,**E**,**H**) and angle of polarization α (**C**,**F**,**I**) of Lake Balaton at the harbour of Balatonfenyves (46°42′39″N, 17°28′40″E) measured with drone-based imaging polarimetry in the blue (450 nm) spectral range from three different heights (h = 232, 165, 232 m) and azimuth angles ($\beta = -29.9°$, +56.4°, +86.3° clockwise from the solar meridian) of the drone's optical axis on 3 May 2022 at 12:30:54, 12:36:17, and 12:32:42 (=UTC + 2 h), respectively. In the α-patterns the white bars show the local directions of polarization.

Since our polarization camera was a simultaneous imaging polarimeter (taking the four polarization images at once with a shutter period of 20 µs), practically no motion/change artefacts occurred in the evaluated polarization patterns. Therefore, the ever-moving surface waves (if any) were captured in situ and in the moment. Since both the degree d and angle α of polarization of reflected light depended on the incident angle, the water waves were more or less discernible in a given polarization pattern, depending on their wavelength and amplitude. However, we performed our three polarimetric campaigns

under almost windless conditions, therefore on the lake surface there were only small (short and tiny amplitude) waves (ripples) generated by local breezes. Therefore, water waves were only slightly discernible in the polarization patterns of Figures 5–8 (and Supplementary Figures S1–S8). Consequently, these patterns were practically the same as those of the corresponding flat, waveless lake surface. On the other hand, in cases of a surface wave that was shorter than the image resolution of our polarization camera, a sensor subpixel averaged the d- and α-values changing spatially along the wave, which inevitably resulted in a slightly reduced d. In our cases, however, this was not a serious problem owing to the calm weather circumstances during our measurements. Thus, water waves had only a negligible impact on the polarization results presented in this work.

Since the optical axis of our polarization camera with angular diameter δ of its field of view was tilted by the Brewster's angle $\theta_{Brewster}$ from the vertical, the topmost and bottommost subpixels in the circular images of Figures 5–8 (and Supplementary Figures S1–S8) had incident angles $\gamma_{topmmost} = \theta_{Brewster} + \delta/2 = 96^\circ$ and $\gamma_{bottommost} = \theta_{Brewster} - \delta/2 = 10^\circ$ measured from the vertical on the horizontal water surface (Figure 4). Since the d of water-reflected light is maximal at $\theta_{Brewster}$ and it decreases with increasing deviation from this direction of view, in the circular d-patterns of Figures 5–8 (and Supplementary Figures S1–S8) the d of the lake surface tendentiously decreased vertically away from the horizontal diameter. On the other hand, in Figures 5–8 (and Supplementary Figures S1–S8), the incident angle on the water surface decreased horizontally only slightly away from the vertical diameter; thus, the d of the lake surface changed horizontally only slightly owing to the wide field of view. These changes of d were not monotonous because of (i) the spatially changing water darkness from the dark water flowing into the bright lake water, and (ii) the mirroring of clouds.

One of the consequences of the above was that in the lowermost regions of the lake surface of Figures 5D,G,J, 6F,I, 7F and 8C,F,I the angle of polarization α was approximately vertical ($\alpha \approx 0^\circ$) and the degree of polarization d was very small ($d < 5\%$) because there the polarization camera looked nearly vertically (incident angle $\gamma_{bottommost} = \theta_{Brewster} - \delta/2 = 10^\circ$ from the vertical) onto the water surface (Figure 4). Here a polarization neutral point occurred (see later).

3.1. Polarimetry at Balatonmariafurdo

Figure 5 (and Supplementary Figures S1 and S2) shows the full optical information (colour picture, radiance I, degree of linear polarization d, and angle of polarization α) of the harbour of Balatonmariafurdo at Lake Balaton measured from the height h = 232 m in the red (650 nm), green (550 nm), and blue (450 nm) spectral ranges available to the drone polarimetry. Figure 6 displays the colour picture as well as the d- and α-patterns of Lake Balaton at the harbour of Balatonmariafurdo measured with drone polarimetry in the blue (450 nm) spectral range from three different heights (h = 156, 232, 236 m) and azimuth angles ($\beta = -22.5^\circ, +26.1^\circ, +84.1^\circ$ clockwise from the solar meridian) of the drone's optical axis. The water between the two parallel concrete walls of the yacht harbour was practically black owing to the inflowing creek water containing black organic matter. In the visible spectrum, this dark-coloured water reflected the light with a high degree of polarization d at the Brewster's angle: d was highest in the blue ($d \leq 80\%$) and lowest in the red ($d \leq 60\%$). The direction (i.e., angle α) of polarization of light reflected by the dark-coloured water was practically horizontal ($\alpha \approx \pm 90^\circ$ from the vertical). The small deviations from the horizontal were due to the perspective in the wide field of view of the polarization camera.

At the outflowing end of the harbour, the mixing of the black harbour water and the bright lake water resulted in a transient, dark, greenish grey area with a gradually decreasing darkness and degree of polarization with increasing distance from the harbour's end (Figures 5 and 6 and Supplementary Figures S1 and S2). However, the angle of polarization of this dark patch remained horizontal in all three (R, G, B) spectral ranges. Farther from this dark patch, the bright lake water reflected horizontally polarized light with low degrees of polarization ($d \leq 20\%$). In the lower middle region of the field of view

a polarization neutral point occurred with zero degree of polarization (d = 0%) where the angle of polarization switched from horizontal to vertical, i.e., the angle of polarization α changed from 90° to 0° (Figures 5C,D,F,G,I,J and 6E,F,H,I).

While the α-pattern was practically independent of the wavelength λ of light, the d-pattern depended on λ (Figure 5 and Supplementary Figures S1 and S2) as mentioned. The far clouds were reflected from the further areas of the water surface. These reflecting clouds made the radiance pattern of the water surface patchy; therefore, both the d- and α-patterns were also more or less patchy (Figures 5 and 6).

3.2. Polarimetry at the Estuary of River Zala

Figure 7 (and Supplementary Figures S3–S5) shows the colour picture as well as the d- and α-patterns of Lake Balaton at the estuary of the River Zala measured with drone polarimetry in the blue (450 nm) spectral range from heights h = 116, 234, 235 m and β = −38.2°, −40.0°, +117.9° azimuth angles clockwise from the solar meridian. River Zala has nearly black water (Figure 7A) because of the dissolved black organic matter. Because of this blackness, the degree of polarization of river-reflected light was very high ($d \leq 80\%$) at the Brewster's angle (Figure 7B) with horizontal polarization (Figure 7C). This highly polarizing black river water flows into the lake where it mixes with the bright and weakly polarizing lake water. Thus, in the estuary an elongated track of mixed water forms with gradually decreasing darkness (because of the gradual dilution, Figure 7D,G) and degree of polarization (Figure 7E,H), but keeping its horizontal polarization (Figure 7F,I). The large contrast in both the radiance and the degree of polarization was well observable between the darker mixed water and the brighter lake water (Figure 7D,E,G,H), while there was no such contrast in the angle of polarization (Figure 7F,I). The α-pattern was again practically independent of the wavelength λ of light (Supplementary Figures S3–S5).

3.3. Polarimetry at Balatonfenyves

Figure 8 (and Supplementary Figures S6–S8) represents the colour picture as well as the d- and α-patterns of Lake Balaton at the yacht harbour of Balatonfenyves measured with drone polarimetry in the blue (450 nm) part of the spectrum from heights h = 232, 165, 232 m and with azimuth angles β = −29.9°, +56.4°, +86.38° clockwise from the solar meridian. In Balatonfenyves, the greenish middle grey harbour water was not as dark (black) as that at Balatonmariafurdo (Figures 5 and 6 and Supplementary Figures S1 and S2) and the water of the River Zala (Figure 7 and Supplementary Figures S3–S5). The consequence of the much lower darkness of the harbour water at Balatonfenyves was its much lower polarizing capability ($d \leq 30\%$) (Figure 8B,E,H). In Figure 8A,G the centre of the brightest sun patch was overexposed, while its annular periphery was highly polarizing ($d \leq 70\%$) (Figure 8B,H), because at Brewster's angle the horizontally polarized intense sunlight overwhelmed the vertically polarized much weaker light coming from below the water surface. At Balatonfenyves, most of the water surface was again horizontally polarizing (Figure 8C,F,I), and the α-pattern was nearly independent of the wavelength (Supplementary Figures S6–S8). Furthermore, in the lower middle region of the field of view, a polarization neutral point occurred (Figure 8B,C,E,F,H,I).

3.4. Influence of Specular Reflection

In Figures 5, 6 and 8 (and Supplementary Figures S1, S6 and S8) quite bright patches occur on the lake surface from which direct sunlight was specularly reflected. Although the sun is not visible in these figures, these bright patches occurred owing to water ripples making the water surface rough, and thus, sunlight could be specularly reflected to the field of view of the camera from the curved surface of ripples. The central spot of these patches was too bright, therefore it was overexposed. In spite of this central overexposure, it was clearly seen that the annular periphery of these bright patches was highly polarized (d > 40–50%) with the angle of polarization perpendicular to the scattering plane determined by the sun, the observer (the polarization camera), and the point observed. The reason for the high d of

these bright lake patches was that the radiance I of the vertically polarized refracted light coming from water was much less than the I of the highly polarized sunlight reflected specularly from the water surface, and thus, the former component decreased only slightly the high d of the latter component. If from a given viewing direction the angle of polarization of such a bright patch is not horizontally polarized, then a flying polarotactic aquatic insect does not sense it as water surface and thus is not attracted by it in spite of its high d.

4. Discussion

We obtained that the degree of polarization d of water-reflected light was highest in the blue ($d \leq 80\%$) and lowest in the red ($d \leq 60\%$) spectral range. The reason for this was that the incident blue skylight was the most/least intense in the blue/red part of the spectrum, and thus, the partially horizontally polarized light reflected from the water surface was also the most/least intense in the blue/red. Consequently, the partially vertically polarized light coming from water could decrease the net degree of polarization the least/most in the blue/red spectral range.

4.1. Advantages of Drone-Based Imaging Polarimetry

Imaging drone polarimetry is a novel method that provides the opportunity to perform new types of measurements. It can also be used, for example, to measure the reflection-polarization patterns of water surfaces that can only be approached from the air. Such surfaces are, for instance, the smaller open water parts of large backwaters covered with floating seaweed vegetation, which are of great importance because they indicate the wetland for flying aquatic insects from a long distance with the horizontally polarized light reflected from their surface [28]. It is a well-known phenomenon that the colour of water bodies and the polarizing capability of water surfaces can change owing to the overgrowth of certain algae and bacteria [29]. Drone polarimetry is an ideal tool for examining these periodic changes.

The reflection-polarization characteristics of water bodies are of great relevance in the water-detection ability of aquatic insects by means of the horizontal polarization of water-reflected light [30]. Until now, the reflection-polarization patterns of various water bodies have been measured by ground-borne imaging polarimetry: Using video polarimetry, Horváth and Varjú [31], for example, measured the polarization patterns of freshwater habitats and pointed out their relevance for water detection by aquatic insects. Gál et al. [32] measured the reflection-polarization patterns of the flat water surface under a clear sky at sunset and compared them to those calculated theoretically using Fresnel's laws of polarization. Csabai et al. [33] studied the reflection-polarization patterns of dark and bright water-imitating horizontal reflectors versus the solar elevation angle and explained why water-seeking aquatic insects fly predominantly in the morning, at noon, and in the evening. By this they discovered the polarization sun dial of dispersing aquatic insects.

4.2. Ecological Implication: Relationship between Measured Polarization and Aquatic Insects

For water-seeking, flying polarotactic aquatic insects, the only relevant information is the reflection-polarization characteristics of water-reflected light, and we omitted to describe in detail the polarization features of the terrestrial coastline of Lake Balaton. The sky was also visible in the wide field of view of our drone-based polarization camera. We mentioned only that the coastline and other non-shiny (i.e., matte) terrestrial objects are usually much less polarized ($d < 15\%$) than water surfaces. The degree of polarization d of sky light depends strongly on the viewing direction relative to the sun and the occurrence of depolarizing clouds [34]. The angle of polarization of light reflected from terrestrial surfaces or originating from the sky generally deviates from the horizontal. These terrestrial and celestial polarization characteristics are not of interest when exploring the viewpoint of a polarotactic aquatic insect attracted only to horizontally polarized light with a high enough d. Although the polarization behaviour of a flat water surface is rather simple and can be calculated by the Fresnel equations [30,32], the reflection-polarization patterns of real

water surfaces [28] should be measured rather than calculated because of their complexity, as demonstrated also in this work (Figures 5–8, Supplementary Figures S1–S8).

Aquatic insects detect water by means of positive polarotaxis, that is, by the horizontal polarization of water-reflected light, if its degree of polarization d is higher than a species-specific threshold d^* [7,8]. For these insects, light with a high enough degree of polarization (i.e., $d > d^*$), the angle of polarization α (measured clockwise from the vertical) of which deviates from the horizontal ($\alpha = 90^\circ$) by smaller than a species-specific threshold $\Delta\alpha$ (i.e., $|\alpha - 90^\circ| < \Delta\alpha$), means water [19]. It is a general rule that the higher the d, the larger is the attractiveness of (nearly) horizontally polarized light to water-seeking aquatic insects [9,10,19–22]. Therefore, since the dark lake patches studied in this work reflected exactly or approximately horizontally polarized light with much higher d-values than the brighter lake waters (Figures 5–8, Supplementary Figures S1–S8), these dark patches were much more attractive to polarotactic aquatic insects than the bright lake water. However, it does not matter that aquatic insects are drawn to these dark lake patches, and this cannot be connected to the general insect decline problem.

In this work, we presented the first reflection-polarization patterns of water surfaces measured by drone-based imaging polarimetry. The peculiarity of these lake surfaces is that they contain large dark patches between autumn and spring because the black canal or river water flows into the bright lake water. Artificial horizontal shiny dark surfaces usually function as strong polarized-light-polluting sources for aquatic insects. However, the high degree of horizontal polarization of the light reflected from these dark lake patches is ecologically advantageous: Certain swarming and water-seeking aquatic insects are likely to lay eggs in these dark lake patches because the degree of polarization d of the dark lake water is much higher than the surrounding bright waters. This is optically supported by our reflection-polarization patterns measured by drone polarimetry (Figures 5–8, Supplementary Figures S1–S8). Our drone-based imaging polarimetric measurements demonstrated what water-seeking polarotactic insects perceive when flying over such dark lake patches.

When a water-seeking polarotactic insect flies above the weakly and horizontally polarizing bright water of Lake Balaton, it can also perceive the highly and horizontally polarized light reflected from the dark water surface of the studied harbours or the river estuary. The latter optical signal is very attractive to the insect, which therefore may approach and land in the dark harbour or estuary water, rather than in the bright lake water. The most attractive option is surely the almost black harbour water possessing a maximal degree of polarization. Because of its gradually decreasing degree of polarization, less attractive is the dark water patch next to the harbour's end gate. The least attractive is the bright lake water because of its lowest polarizing capability. Since aquatic insects may prefer the black harbour water and the dark water patch, instead of the bright lake water, they can lay their eggs in the former waters, where their larvae can accumulate. The in situ test of such an accumulation by samplings will be an interesting task for future research.

Such an accumulation of larvae in the dark lake patches can be either advantageous or disadvantageous for the concerned insect population: On the one hand, the black organic matter suspended/dissolved in the black/dark harbour and estuary water could provide enhanced nutrition for the larvae, which is advantageous. On the other hand, the boat/yacht traffic in the harbour can disturb the life/development of larvae, increasing the water pollution (i.e., because of contamination by ship's fuel). Only further ecological studies can reveal the net influence of these advantageous and disadvantageous effects on the accumulated larvae.

Supplementary Materials: The following supporting information can be downloaded at: https://www.mdpi.com/article/10.3390/rs15112797/s1, Figure S1. Colour picture and patterns of the radiance I, degree of linear polarization d, and angle of polarization α of Lake Balaton at the harbour of Balatonmariafurdo (46°42′22″N, 17°22′14″E) measured with drone-based imaging polarimetry from height h = 156 m in the red (650 nm), green (550 nm), and blue (450 nm) spectral ranges on 3 May 2022 at 13:48:13 (=UTC + 2 h). In the α-patterns the white bars show the local directions of

polarization. The azimuth angle of the drone's optical axis is $\beta = -22.5^{o}$ clockwise from the solar meridian. Figure S2. Colour picture and patterns of the radiance I, degree of linear polarization d, and angle of polarization α of Lake Balaton at the harbour of Balatonmariafurdo (46°42′22″N, 17°22′14″E) measured with drone-based imaging polarimetry from height h = 236 m in the red (650 nm), green (550 nm), and blue (450 nm) spectral ranges on 3 May 2022 at 13:42:23 (=UTC + 2 h). In the α-patterns the white bars show the local directions of polarization. The azimuth angle of the drone's optical axis is $\beta = +84.1°$ clockwise from the solar meridian. Figure S3. Colour picture and patterns of the radiance I, degree of linear polarization d, and angle of polarization α of Lake Balaton at the estuary of the River Zala (46°42′21″N, 17°15′53″E) measured with drone-based imaging polarimetry from height h = 116 m in the red (650 nm), green (550 nm), and blue (450 nm) spectral ranges on 3 May 2022 at 15:06:46 (=UTC + 2 h). In the α-patterns the white bars show the local directions of polarization. The azimuth angle of the drone's optical axis is $\beta = -38.2°$ clockwise from the solar meridian. Figure S4. Colour picture and patterns of the radiance I, degree of linear polarization d, and angle of polarization α of Lake Balaton at the estuary of the River Zala (46°42′21″N, 17°15′53″E) measured with drone-based imaging polarimetry from height h = 234 m in the red (650 nm), green (550 nm), and blue (450 nm) spectral ranges on 3 May 2022 at 15:02:14 (=UTC + 2 h). In the α-patterns the white bars show the local directions of polarization. The azimuth angle of the drone's optical axis is $\beta = +40.0^{o}$ clockwise from the solar meridian. Figure S5. Colour picture and patterns of the radiance I, degree of linear polarization d, and angle of polarization α of Lake Balaton at the estuary of the River Zala (46°42′21″N, 17°15′53″E) measured with drone-based imaging polarimetry from height h = 235 m in the red (650 nm), green (550 nm), and blue (450 nm) spectral ranges on 3 May 2022 at 15:00:46 (=UTC + 2 h). In the α-patterns the white bars show the local directions of polarization. The azimuth angle of the drone's optical axis is $\beta = +117.9^{o}$ clockwise from the solar meridian. Figure S6. Colour picture and patterns of the radiance I, degree of linear polarization d, and angle of polarization α of Lake Balaton at the harbour of Balatonfenyves (46°42′39″N, 17°28′40″E) measured with drone-based imaging polarimetry from height h = 232 m in the red (650 nm), green (550 nm), and blue (450 nm) spectral ranges on 3 May 2022 at 12:30:54 (=UTC + 2 h). In the α-patterns the white bars show the local directions of polarization. The azimuth angle of the drone's optical axis is $\beta = -29.9°$ clockwise from the solar meridian. Figure S7. Colour picture and patterns of the radiance I, degree of linear polarization d, and angle of polarization α of Lake Balaton at the harbour of Balatonfenyves (46°42′39″N, 17°28′40″E) measured with drone-based imaging polarimetry from height h = 165 m in the red (650 nm), green (550 nm), and blue (450 nm) spectral ranges on 3 May 2022 at 12:36:17 (=UTC + 2 h). In the α-patterns the white bars show the local directions of polarization. The azimuth angle of the drone's optical axis is $\beta = +56.4°$ clockwise from the solar meridian. Figure S8. Colour picture and patterns of the radiance I, degree of linear polarization d, and angle of polarization α of Lake Balaton at the harbour of Balatonfenyves (46°42′39″N, 17°28′40″E) measured with drone-based imaging polarimetry from height h = 232 m in the red (650 nm), green (550 nm), and blue (450 nm) spectral ranges on 3 May 2022 at 12:32:42 (=UTC + 2 h). In the α-patterns the white bars show the local directions of polarization. The azimuth angle of the drone's optical axis is $\beta = +86.3°$ clockwise from the solar meridian.

Author Contributions: Substantial contributions to conception and design: D.S., P.T., B.B., G.K., A.B., I.P. and G.H.; software development: D.S., P.T., A.B. and I.P.; experiments and measurements: D.S., P.T., B.B. and G.K.; data visualisation: D.S., P.T., A.B., I.P. and G.H.; data analysis and interpretation: D.S., P.T., G.K. and G.H.; drafting and revising the article critically: D.S., P.T., G.K. and G.H. All authors have read and agreed to the published version of the manuscript.

Funding: This research was supported by a KDP-2020-ELTE-1010099 fellowship/grant from the Hungarian National Research, Development and Innovation Office to Péter Takács, who received further financial support from the Doctoral School of the Physical Institute of the Eötvös Loránd University. Dénes Száz was supported by the Hungarian UNKP-21-4 New National Excellence Program of the Ministry for Innovation and Technology from the National Research, Development and Innovation Fund.

Data Availability Statement: All data underlying the results presented in this paper are available in the paper and its Electronic Supplementary Material.

Acknowledgments: We are grateful to two anonymous reviewers for their valuable and constructive comments about earlier versions of our manuscript.

Conflicts of Interest: The authors declare no conflict of interest.

References

1. Schwind, R. A polarization-sensitive response of the flying water bugNotonecta glauca to UV light. *J. Comp. Physiol. A* **1983**, *150*, 87–91. [CrossRef]
2. Schwind, R. Zonation of the optical environment and zonation in the rhabdom structure within the eye of the backswimmer, Notonecta glauca. *Cell Tissue Res.* **1983**, *232*, 53–63. [CrossRef] [PubMed]
3. Schwind, R. Evidence for true polarization vision based on a two-channel analyser system in the eye of the water bug, Notonecta glauca. *J. Comp. Physiol. A* **1984**, *154*, 53–57. [CrossRef]
4. Schwind, R. The plunge reaction of the backswimmerNotonecta glauca. *J. Comp. Physiol. A* **1984**, *155*, 319–321. [CrossRef]
5. Schwind, R. A further proof of polarization vision ofNotonecta glauca and a note on threshold intensity for eliciting the plunge reaction. *Cell. Mol. Life Sci.* **1985**, *41*, 466–467. [CrossRef]
6. Schwind, R. A variety of insects are attracted to water by reflected polarized light. *Sci. Nat.* **1989**, *76*, 377–378. [CrossRef]
7. Schwind, R. Polarization vision in water insects and insects living on a moist substrate. *J. Comp. Physiol. A* **1991**, *169*, 531–540. [CrossRef]
8. Schwind, R. Spectral regions in which aquatic insects see reflected polarized light. *J. Comp. Physiol. A* **1995**, *177*, 439–448. [CrossRef]
9. Wildermuth, H. Dragonflies Recognize the Water of Rendezvous and Oviposition Sites by Horizontally Polarized Light: A Behavioural Field Test. *Sci. Nat.* **1998**, *85*, 297–302. [CrossRef]
10. Wildermuth, H. Polarotaktische Reaktionen von Coenagrion puella und Libellula quadrimaculata auf Erdbeerkulturen als ökologische Falle (Odonata: Coenagrionidae, Libellulidae). *Libellula* **2007**, *26*, 143–150.
11. Boda, P.; Csabai, Z. Seasonal and diel flight activity patterns of aquatic Coleoptera and Heteroptera. *Verh. Der Int. Ver. Für Limnol.* **2009**, *30*, 1271–1274. [CrossRef]
12. Boda, P.; Csabai, Z. Seasonal and diel dispersal activity characteristics of *Sigara lateralis* (Leach, 1817) (Heteroptera: Corixidae) with special emphasis on possible environmental factors and breeding state. *Aquat. Insects* **2009**, *31*, 301–314. [CrossRef]
13. Boda, P.; Csabai, Z. When do beetles and bugs fly? A unified scheme for describing seasonal flight behaviour of highly dispersing primary aquatic insects. *Hydrobiologia* **2012**, *703*, 133–147. [CrossRef]
14. Turcsányi, I.; Szentkirályi, F.; Bernáth, B.; Kádár, F. Flight of mayflies towards horizontally polarised and unpolarised light. *Aquat. Insects* **2009**, *31*, 301–310. [CrossRef]
15. Csabai, Z.; Kálmán, Z.; Szivák, I.; Boda, P. Diel flight behaviour and dispersal patterns of aquatic Coleoptera and Heteroptera species with special emphasis on the importance of seasons. *Naturwissenschaften* **2012**, *99*, 751–765. [CrossRef]
16. Horváth, G.; Kriska, G.; Robertson, B. Anthropogenic Polarization and Polarized Light Pollution Inducing Polarized Ecological Traps. In *Polarized Light and Polarization Vision in Animal Sciences*; Chapter 20; Horváth, G., Ed.; Springer: Heidelberg, Germany, 2014; pp. 443–513. [CrossRef]
17. Bernáth, B.; Meyer-Rochow, V.B. Optomotor reactions reveal polarization sensitivity in the Zika virus transmitting yellow fever mosquito Aedes (Stegomyia) aegypti (Diptera; Nematocera). *Zool. Sci.* **2016**, *33*, 643–649. [CrossRef] [PubMed]
18. Ensaldo-Cárdenas, A.S.; Rocha-Ortega, M.; Schneider, D.; Robertson, B.A.; Córdoba-Aguilar, A. Ultraviolet polarized light and individual condition drive habitat selection in tropical damselflies and dragonflies. *Anim. Behav.* **2021**, *180*, 229–238. [CrossRef]
19. Horváth, G.; Csabai, Z. Polarization Vision of Aquatic Insects. In *Polarized Light and Polarization Vision in Animal Sciences*; Chapter 5; Horváth, G., Ed.; Springer: Heidelberg, Germany, 2014; pp. 113–145.
20. Horváth, G.; Zeil, J. Kuwait oil lakes as insect traps. *Nature* **1996**, *379*, 303–304. [CrossRef]
21. Bernáth, B.; Szedenics, G.; Molnár, G.; Kriska, G.; Horváth, G. Visual ecological impact of 'shiny black anthropogenic products' on aquatic insects: Oil reservoirs and plastic sheets as polarized traps for insects associated with water. *Arch. Nat. Conserv. Landsc. Res.* **2001**, *40*, 89–109.
22. Kriska, G.; Horváth, G.; Andrikovics, S. Why do mayflies lay their eggs en masse on dry asphalt roads? Water-imitating polarized light reflected from asphalt attracts Ephemeroptera. *J. Exp. Biol.* **1998**, *201*, 2273–2286. [CrossRef]
23. Robertson, B.; Chalfoun, A. Evolutionary traps as keys to understanding behavioral maladapation. *Curr. Opin. Behav. Sci.* **2016**, *12*, 12–17. [CrossRef]
24. Robertson, B.A.; Blumstein, D.T. How to disarm an evolutionary trap. *Conserv. Sci. Pract.* **2019**, *1*, e116. [CrossRef]
25. Black, T.V.; Robertson, B.A. How to disguise evolutionary traps created by solar panels. *J. Insect Conserv.* **2019**, *24*, 241–247. [CrossRef]
26. Fraleigh, D.C.; Heitmann, J.B.; Robertson, B.A. Ultraviolet polarized light pollution and evolutionary traps for aquatic insects. *Anim. Behav.* **2021**, *180*, 239–247. [CrossRef]
27. Haynes, K.J.; Robertson, B.A. A transdisciplinary research agenda for understanding insect responses to ecological light pollution informed by evolutionary trap theory. *Curr. Opin. Insect Sci.* **2021**, *45*, 91–96. [CrossRef] [PubMed]
28. Horváth, G. Polarization patterns of freshwater bodies with biological implications. In *Polarized Light and Polarization Vision in Animal Sciences*; Horváth, G., Ed.; Springer: Heidelberg, Germany, 2014; Chapter 16; pp. 333–344.
29. Tingting, T.; Yingxiao, M.; Wendi, S.; Li, Z.; Dai, R.; Ye, J. Effects of algae on the formation of black blooms and bacterial community structure changes in sediments and black floats. *Water* **2022**, *14*, 2348. [CrossRef]

30. Schwind, R.; Horváth, G. Reflection-polarization pattern at water surfaces and correction of a common representation of the polarization pattern of the sky. *Naturwissenschaften* **1993**, *80*, 82–83. [CrossRef]
31. Horváth, G.; Varjú, D. Polarization pattern of freshwater habitats recorded by video polarimetry in red, green and blue spectral ranges and its relevance for water detection by aquatic insects. *J. Exp. Biol.* **1997**, *200*, 1155–1163. [CrossRef]
32. Gál, J.; Horváth, G.; Meyer-Rochow, V.B. Measurement of the reflection-polarization pattern of the flat water surface under a clear sky at sunset. *Remote Sens. Environ.* **2001**, *76*, 103–111. [CrossRef]
33. Csabai, Z.; Boda, P.; Bernáth, B.; Kriska, G.; Horváth, G. A 'polarisation sun-dial' dictates the optimal time of day for dispersal by flying aquatic insects. *Freshw. Biol.* **2006**, *51*, 1341–1350. [CrossRef]
34. Horváth, G.; Barta, A.; Hegedüs, R. Chapter 18: Polarization of the Sky. In *Polarized Light and Polarization Vision in Animal Sciences*; Horváth, G., Ed.; Springer: Heidelberg, Germany, 2014; pp. 367–406.